Domingo-Sananes et al., http://www.jcb.org/cgi/content/full/jcb.201506114/DC1

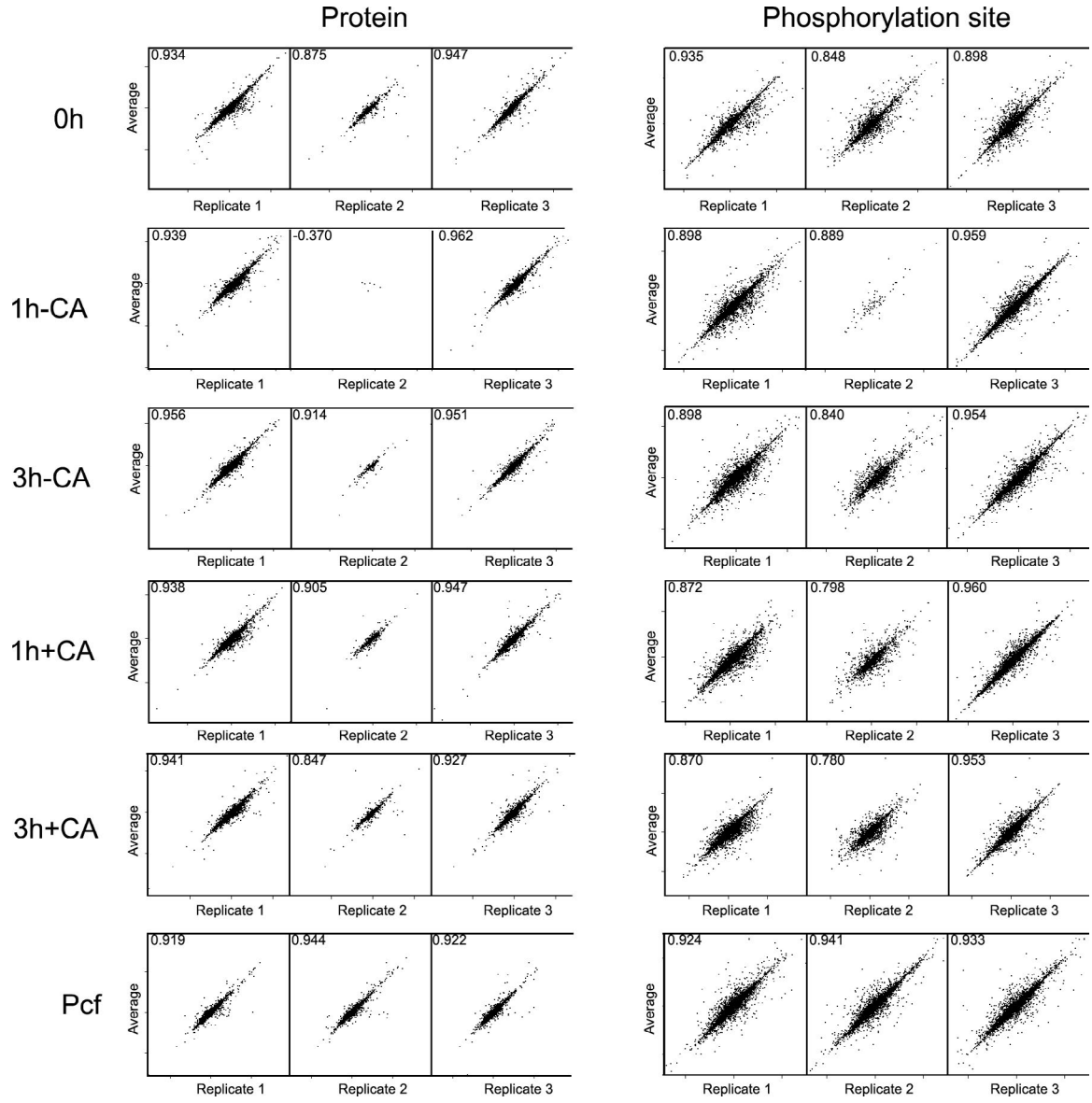

Figure S1. **Reproducibility of the proteomic analysis.** Comparison of the SILAC H/L ratio of individual biological replicates to the mean SILAC H/L ratio (with Pearson correlation). Protein data are on the left and phosphorylation site data are on the right, with each row representing different experimental regimens: 0 h – stumpy, *t* = 0 h; 1 h – CA, *t* = 1 h no CA; 3 h – CA, *t* = 3 h no CA; 1 h + CA, *t* = 1 h with CA; and 3 h + CA, *t* = 3 h with CA. Pcf, cultured procylic form cell.

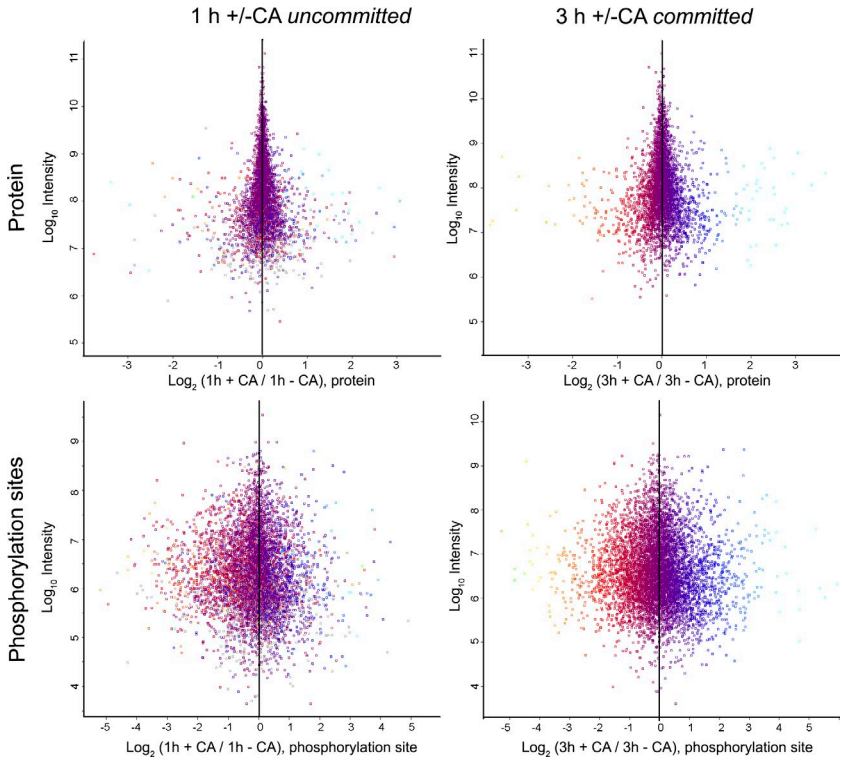

Figure S2. **Changes in proteome and phosphoproteome in response to CA treatment.** Changes before (1 h) and after (3 h) commitment were quantified by comparing treated and untreated samples at each time point, using the heavy isotope–labeled standard as an internal control. Changes in phosphorylation sites are larger and occur earlier than changes in protein abundance.

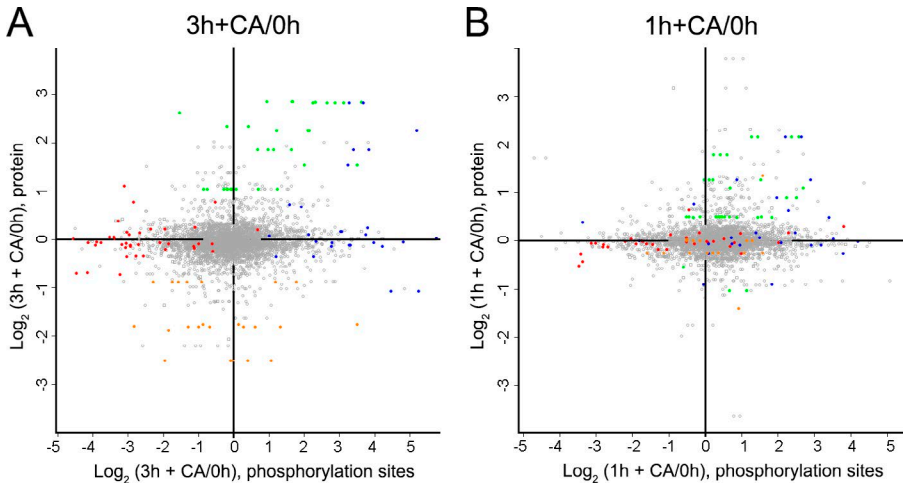

Figure S3. **Observed changes in the proteome are driven by changes induced by CA treatment.** Changes in protein and phosphorylation site abundance in the cells treated with CA for 1 and 3 h compared with untreated cells at time zero. Coloring represents the greatest changes that occur at 3 h + CA/3 h − CA (as Fig. 7 A), defined as follows: blue, phosphorylation site up at 3 h + CA ($\log_2$ [3 h + CA/3 h − CCA], phosphorylation site ≥ 3.0); red, phosphorylation sites down 3 h + CA ($\log_2$ [3 h + CA/3 h − CCA], phosphorylation site ≤ −3.0); green, proteins up 3 h + CA ($\log_2$ [3 h + CA/3 h − CCA], protein ≥ 1.5); and orange, proteins down 3 h + CA ($\log_2$ [3 h + CA/3 h − CA], protein ≤ −1.5).

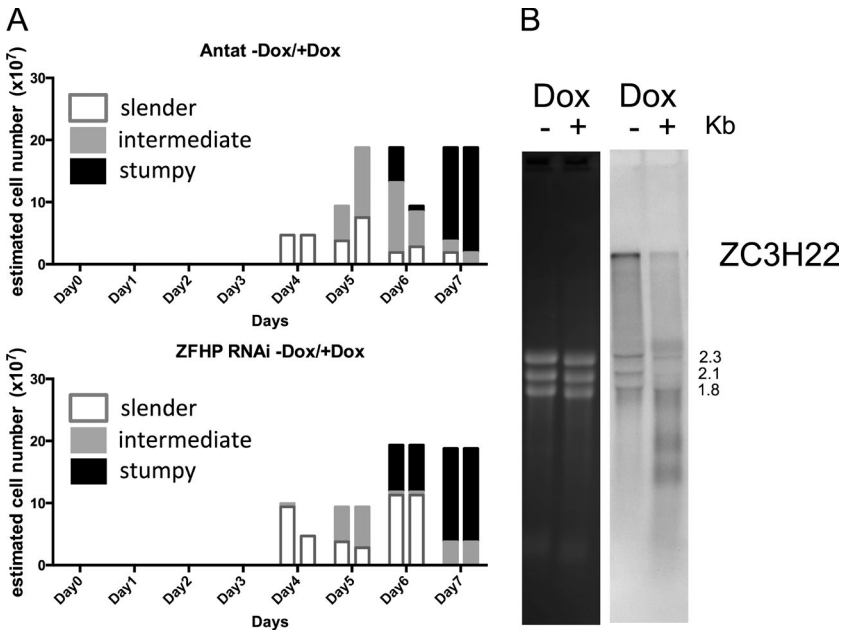

Figure S4. **In vivo growth of ZC3H22 RNAi lines and Northern blot of the ZC3H22 transcript after RNAi.** (A) A pleomorphic RNAi line depleting the ZC3H22 transcript was generated and analyzed for its growth in vivo. The parasites grew at an equivalent level and progressed from slender to stumpy forms on an equivalent timescale. The in vivo analysis was performed once with $n = 250$ cells per time point analyzed. In vitro growth analyses of four independent RNAi lines also demonstrated an absence of growth effect upon ZC3H22 depletion. (B) Northern blotting for the ZC3H22 transcript demonstrated depletion of the mRNA upon RNAi induction. Dox, doxycycline.

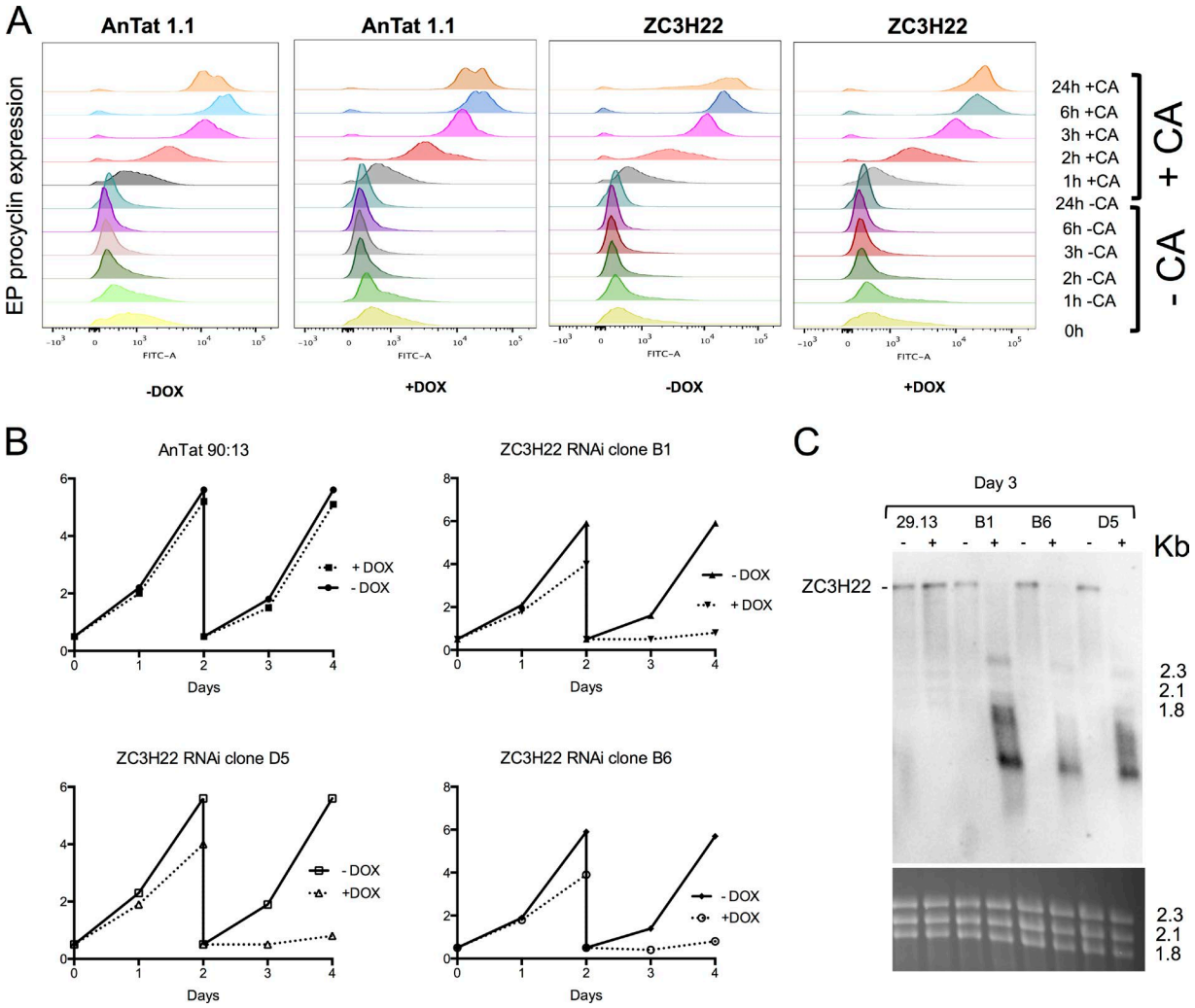

Figure S5. **ZC3H22 is required for procyclic form viability but not differentiation.** (A) Stumpy forms depleted of ZCH22 by RNAi after growth in doxycycline (DOX)–treated mice were harvested as enriched stumpy form populations and then incubated in vitro in the presence or absence of CA. No differentiation occurred in the absence of CA; with CA, the parasites expressed EP procyclin as a differentiation marker with kinetics equivalent to the parental AnTat1.1 90:13 line. The in vivo analyses were performed once; four independent lines were also analyzed in vitro, each generating no effect upon differentiation when ZC3H22 depletion was induced. (B) Three independently derived RNAi lines for ZC3H22 in procyclic forms demonstrated growth inhibition upon RNA induction with doxycycline. Control AnTat90:13 procyclic cells did not show growth inhibition in the presence of doxycycline. (C) Northern blot showing the depletion of the ZC3H22 transcript in each of three independent procyclic form RNAi lines. The RNAs were prepared after 72-h induction with tetracycline.

Table S1. **PTP1 regulated phosphotyrosine site**

TriTrypDB ID	Product	pY site	Sequence	Comment
Tb927.9.6090	PIP39, PTP1-interacting protein	Y278	ADEpYTK	<7–amino acid cutoff
Tb927.9.6100	PIP39, PTP1-interacting protein	Y278	ADEpYTK	<7–amino acid cutoff
Tb927.8.760	NOPP44/46, nucleolar RNA binding protein	Y181	DAGDEDDNDDDEApYDEDDSDDDDDDD DDDDDDDDDDDDE	Too acidic

Provided online are Tables S2–S4. Table S2 shows quantitative proteomic analysis of commitment to differentiation. Table S3 shows quantitative phosphoproteomic analysis of commitment to differentiation. Table S4 shows phosphorylation sites observed only in the "light" experimental samples analysis.

References

Alsford, S., D.J. Turner, S.O. Obado, A. Sanchez-Flores, L. Glover, M. Berriman, C. Hertz-Fowler, and D. Horn. 2011. High-throughput phenotyping using parallel sequencing of RNA interference targets in the African trypanosome. *Genome Res.* 21:915–924. http://dx.doi.org/10.1101/gr.115089.110

Erben, E.D., A. Fadda, S. Lueong, J.D. Hoheisel, and C. Clayton. 2014. A genome-wide tethering screen reveals novel potential post-transcriptional regulators in *Trypanosoma brucei. PLoS Pathog.* 10:e1004178.

Fadda, A., M. Ryten, D. Droll, F. Rojas, V. Färber, J.R. Haanstra, C. Merce, B.M. Bakker, K. Matthews, and C. Clayton. 2014. Transcriptome-wide analysis of trypanosome mRNA decay reveals complex degradation kinetics and suggests a role for co-transcriptional degradation in determining mRNA levels. *Mol. Microbiol.* 94:307–326. http://dx.doi.org/10.1111/mmi.12764

Güther, M.L., M.D. Urbaniak, A. Tavendale, A. Prescott, and M.A. Ferguson. 2014. High-confidence glycosome proteome for procyclic form *Trypanosoma brucei* by epitope-tag organelle enrichment and SILAC proteomics. *J. Proteome Res.* 13:2796–2806. http://dx.doi.org/10.1021/pr401209w

Parsons, M., E.A. Worthey, P.N. Ward, and J.C. Mottram. 2005. Comparative analysis of the kinomes of three pathogenic trypanosomatids: Leishmania major, Trypanosoma brucei and Trypanosoma cruzi. *BMC Genomics.* 6:127. http://dx.doi.org/10.1186/1471-2164-6-127

Shimogawa, M.M., E.A. Saada, A.A. Vashisht, W.D. Barshop, J.A. Wohlschlegel, and K.L. Hill. 2015. Cell surface proteomics provides insight into stage-specific remodeling of the host-parasite interface in *Trypanosoma brucei. Mol. Cell. Proteomics.* 14:1977–1988. http://dx.doi.org/10.1074/mcp.M114.045146